Acta Mechanica 123, 37–56 (1997)

ACTA MECHANICA

On the parameter identification problem for failure criteria in anisotropic bodies

P. S. Theocaris, Athens, and **C. Bisbos** and **P. D. Panagiotopoulos,** Thessaloniki, Greece

(Received May 28, 1996)

Summary. The elliptic paraboloid failure surface criterion (EPFS) is adopted in this paper to describe the failure behaviour of anisotropic bodies. A method is described, based on an inequality-constrained least square problem for the determination of the parameters of the EPFS criterion. After the discussion of the influence of the strength differential effect on the failure behaviour of the material, a neural network learning approach is introduced to the problem of extrapolating the given experimental results beyond the given range of experimental data by establishing an appropriate law of evolution of the failure surface valid for the material up to fracture.

1 Introduction

We consider failure criteria in the 3D-principal stress space, which are appropriate for the description of the failure behaviour of anisotropic bodies, by taking into account the strength differential effect (SDE) along the instantaneous principal stress axes. The general form of any failure criterion is a polynominal of the stress tensor. Among the different criteria we choose here the elliptic paraboloid failure surface criterion (EPFS), which has been extensively studied by [1] and describes satisfactorily the failure properties of anisotropic materials. For the general properties of the EPFS we refer to [2]. Note that a tensor polynomial criterion is represented by hypersurfaces in the stress space and thus it is difficult to be visualized geometrically. Certain plane sections of these hypersurfaces can be plotted, thus offering a maximum visualization of the failure surface. However, these plane sections do not yield a direct information on the relations of the material strength in a prescribed direction to the externally applied load on the specimen under consideration. This fact constitutes a drawback of the tensor polynomial criteria generally. Therefore, one needs until now delicate experimentation and an extensive stochastic analysis based e.g. on Weibull's distribution theory [2], in order to identify with acceptable accuracy the values of the parameters of the failure polynomial.

Here we present another method, which avoids the meticulous experimentation and the use of probabilistic tools. The method we present is based on an extension of the least square problem and identifies the coefficients of the tensor polynomial failure criterion, here the EPFS-criterion. The original part of the method is the consideration of an inequality constrained version of the least square approach to the identification problem, which by means of the additional inequality constraints takes into account important information of the physical problem. The result in the calculations is the straightforward determination of the unknown coefficients by means of a quadratic programming algorithm. The method is stable and its accuracy can be improved as much as one wants, but in the limits of the measurement accuracy.

Further, we discuss the influence of the SDE on the form of the EPFS by giving, for a series of experiments, the variations of the corresponding curves-intersections of the EPFS by certain planes of the principal stress space. In order to have a picture of the failure surface changes for loading paths between the given or beyond the given ones, we propose a method based on a neural-network supervised learning algorithm, which permits the interpolation and the extrapolation of the given failure surfaces. The prediction of the material behaviour in the future loading combinations results from the network learning algorithm and is based on simple but long iterative calculations. In this respect we refer also to [3]–[7].

2 The elliptic paraboloid failure surface

The elliptic paraboloid failure surface was introduced by the first author, first in order to describe the failure of isotropic materials for which the EPFS is reduced to a paraboloid of revolution. For ***anisotropic*** materials the EPFS depends mainly on the six strength parameters, three for tension and three for compression, along the principal strength axes of the material. It was shown that the three strength differential factors σ_{Ci}/σ_{Ti}, $i = 1, 2, 3$ (C means compression and T means tension) characterize mainly the variation of the EPFS with loading. The failure condition, expressed in terms of principal stress components, σ_i, has the general form of the quadric surface equation, that is:

$$H_{ij}\sigma_i\sigma_j + h_i\sigma_i - 1 = 0 \quad (i,j = 1, \ldots, 3) \tag{2.1}$$

where the tensor H_{ij} and the vector h_i are appropriately defined in terms of the basic strength properties of the material. Such a formulation of the anisotropic failure criterion is restricted to a material symmetry up to orthotropy at most.

Then, the quadric surface equation (2.1), if written in terms of the Cartesian components of the stress tensor, takes the following form:

$$f(\boldsymbol{\sigma}) = \boldsymbol{\sigma} \cdot \boldsymbol{H} \cdot \boldsymbol{\sigma} + \boldsymbol{h} \cdot \boldsymbol{\sigma} - 1 = 0 \tag{2.2}$$

where $\boldsymbol{H}$ and $\boldsymbol{h}$ denote 4^{th} and 2^{nd}-rank *failure tensors* respectively. Thus (2.2) shows the existence of a safe triaxial loading path, which means that the failure hypersurface must not be intersected by some stress-tensor direction. For isotropic materials it is generally accepted and experimentally proved that the hydrostatic loading constitutes safe triaxial loading path. For anisotropic materials this safe triaxial loading path is parallel displaced by a well defined distance taking into account the influence of anisotropy.

The values of the failure function $f(\boldsymbol{\sigma})$ for the initially anisotropic elastic solid with respect to the tensor $\boldsymbol{\sigma}$ must be path independent as long as the material does not fail under the loading mode $\boldsymbol{\sigma}$. Since the stress tensor is considered symmetric, *path independence* of function $f(\boldsymbol{\sigma})$ is guaranteed by the *symmetric failure tensors* $\boldsymbol{H}$ and $\boldsymbol{h}$. The linear polynomial term, $\boldsymbol{h}.\boldsymbol{\sigma}$, accounts for the strength differential effect whereas the failure tensor $\boldsymbol{H}$ accounts for the plasticity effect.

The form of Eq. (2.2) does not impose any restriction on the symmetry class of the anisotropic medium and thus the 4^{th} rank failure tensor $\boldsymbol{H}$ may possess at most 21 independent components. Symmetry properties of tensor $\boldsymbol{H}$ follow those of elastic compliance 4^{th}-rank failure tensor, $\boldsymbol{S}$. The 2^{nd}-rank failure tensor, $\boldsymbol{h}$, may have, in general, six independent components, whereas, for specially orthotropic media, or of increased symmetry, tensor $\boldsymbol{h}$ becomes *axisymmetric* degenerating to a *spherical tensor* for the isotropic medium.

It is shown, e.g. in [2], that the normal components of the failure tensor are expressed by:

$$H_{ii} = \frac{1}{\sigma_{Ti}\sigma_{Ci}} \quad (i \leqq 3) \tag{2.3}$$

$$h_i = \left(\frac{1}{\sigma_{Ti}}\right) - \left(\frac{1}{\sigma_{Ci}}\right) = (\sigma_{Ci} - \sigma_{Ti})\, H_{ii} \tag{2.4}$$

whereas shear components are given by:

$$\begin{aligned} H_{ii} &= \frac{1}{\sigma_{Si}} + \sigma_{Si} \quad (i > 3) \\ h_i &= \left(\frac{1}{\sigma_{Si}^{+}}\right) - \left(\frac{1}{\sigma_{Si}^{-}}\right) = (\sigma_{Si}^{-} - \sigma_{Si}^{+})\, H_{ii}. \end{aligned} \tag{2.5}$$

In the above relations the repeated index convention does not apply and the σ_{Ti} and σ_{Ci}-stresses express the tension (T) and compression (C) failure stresses in the i-direction. Furthermore, the σ_{Si}^{+}, σ_{Si}^{-}-stresses express the shear strengths, positive or negative, in the i-plane ($i > 3$), and the usual contracted notation of Cartesian indices is used, meaning, that index 4 corresponds to natural indices 2, 3, index 5 to 1, 3 and index 6 to 1, 2. For the orthotropic materials, there is no shear-strength differential effect, if the coordinate system coincides with the material symmetry direction and thus $\sigma_{Si}^{+} = \sigma_{Si}^{-}$.

The requirement that the failure hypersurface is an open-end surface is assured by imposing the $\boldsymbol{H}$-tensor to have a zero eigenvalue. The condition that any applied hydrostatic stress should constitute a safe loading path is satisfied by associating the zero eigenvalue of $\boldsymbol{H}$-tensor to the 2nd rank spherical tensor $\mathbf{1}$, which is then an eigentensor of $\boldsymbol{H}$. Then, it should be valid that $\boldsymbol{H} \cdot \mathbf{1} = 0$, a relation which yields, among others, the following three relationships:

$$\begin{aligned} H_{12} &= \frac{1}{2}(H_{33} - H_{11} - H_{22}), \\ H_{23} &= \frac{1}{2}(H_{11} - H_{22} - H_{33}), \\ H_{31} &= \frac{1}{2}(H_{22} - H_{33} - H_{11}). \end{aligned} \tag{2.6}$$

Relations (2.6) imply that the coefficients H_{12}, H_{23} and H_{31} of the EPFS are interrelated with the diagonal components, which are directly defined through the basic strength data. This is a significant advantage of the EPFS-criterion, which is not met with other similar criteria, which either are based on the experimental evaluation of these off-diagonal coefficients, or they are defined arbitrarily, based on some assumptions, [8].

For the complete study of the EPFS three intersections must be determined:

i) The principal diagonal intersections, defined by planes containing one principal stress axis, preferably the strong σ_3-axis, and the bisector of the right angle formed by the remaining principal axes.

ii) The deviatoric π-plane, which is normal to the hydrostatic axis.

iii) The principal stress plane intersections, which are convenient for the study of the mechanical properties of the anisotropic body when thin plates of the material under plane-stress conditions have to be studied.

The EPFS for the orthotropic material is expressed in the $(\sigma_1, \sigma_2, \sigma_3)$-principal stress space by a complete polynomial of the seond degree, where the σ_3-principal direction corresponds to the strongest direction [1], [2]:

$$H_{11}\sigma_1{}^2 + H_{22}\sigma_2{}^2 + H_{33}\sigma_3{}^2 + (H_{33} - H_{11} - H_{22})\,\sigma_1\sigma_2 + (H_{11} - H_{22} - H_{33})\,\sigma_2\sigma_3$$
$$+ (H_{22} - H_{33} - H_{11})\,\sigma_1\sigma_3 + h_1\sigma_1 + h_2\sigma_2 + h_3\sigma_3 = 1. \tag{2.7}$$

This second-degree polynomial, referred to the Cartesian coordinate system $0xyz$, where the 0z-axis is parallel to the hydrostatic axis and the $(0xy)$-plane coincides with the deviatoric plane with the $0y$-axis lying on the $(\sigma_3\delta_{12})$–principal diagonal plane (δ_{12} being the bisector of the $\sigma_1 0\sigma_2$-angle), is expressed by:

$$\left(H_{11} + H_{22} - \frac{1}{2}H_{33}\right)x^2 + 3/2H_{33}y^2 + \sqrt{3}\,(H_{11} - H_{22})\,xy + \frac{1}{2}(h_2 - h_1)\,x$$
$$+ \frac{1}{\sqrt{6}}(2h_3 - h_1 - h_2)\,y + \frac{1}{\sqrt{3}}(h_1 + h_2 + h_3)\,z = 1. \tag{2.8}$$

Moreover, the equation of the intersection of the failure locus and the (σ_3, δ_{12})-plane is given by [1]:

$$\frac{1}{2}(H_{11} + H_{22} + 2H_{12})\,\delta_{12}^2 + H_{33}\sigma_3{}^2 + \sqrt{2}\,(H_{13} + H_{23})\,\delta_{12}\sigma_3$$
$$+ \frac{\sqrt{2}}{2}(h_1 + h_2)\,\delta_{12} + h_3\sigma_3 - 1 = 0. \tag{2.9}$$

Analogous expressions hold for the other intersections.

3 Least square determination of the EPFS coefficients

Let $\boldsymbol{x} \in \mathbb{R}^6$ collect the unknown EPFS coefficients:

$$\boldsymbol{x}^T = (x_1, x_2, x_3, x_4, x_5, x_6)^T = (H_{11}, H_{22}, H_{33}, h_1, h_2, h_3)^T. \tag{3.1}$$

Let $\sigma_1{}^{(i)}, \sigma_2{}^{(i)}, \sigma_3{}^{(i)}$ be the stresses at the i-th measurement point and let further:

$$\begin{aligned}
a_{1i} &= \sigma_1{}^{(i)}\sigma_1{}^{(i)} - \sigma_1{}^{(i)}\sigma_2{}^{(i)} + \sigma_2{}^{(i)}\sigma_3{}^{(i)} - \sigma_3{}^{(i)}\sigma_1{}^{(i)},\\
a_{2i} &= \sigma_2{}^{(i)}\sigma_2{}^{(i)} - \sigma_1{}^{(i)}\sigma_2{}^{(i)} - \sigma_2{}^{(i)}\sigma_3{}^{(i)} + \sigma_3{}^{(i)}\sigma_1{}^{(i)},\\
a_{3i} &= \sigma_3{}^{(i)}\sigma_3{}^{(i)} + \sigma_1{}^{(i)}\sigma_2{}^{(i)} - \sigma_2{}^{(i)}\sigma_3{}^{(i)} - \sigma_3{}^{(i)}\sigma_1{}^{(i)},\\
a_{4i} &= \sigma_1{}^{(i)},\\
a_{5i} &= \sigma_2{}^{(i)},\\
a_{6i} &= \sigma_3{}^{(i)},
\end{aligned} \tag{3.2}$$

collected formally in $\boldsymbol{a}_i \in \mathbb{R}^6$. If the measurement point satisfies the EPFS criterion exactly, then:

$$\boldsymbol{a}_i{}^T\boldsymbol{x} - 1 = 0. \tag{3.3}$$

In general, the measurement error of the i-th point is:

$$e_i = \boldsymbol{a}_i^T \boldsymbol{x} - 1. \tag{3.4}$$

If we have m measurement points, the error vector $e \in \mathbb{R}^m$ will be:

$$\boldsymbol{e} = \boldsymbol{A}^T \boldsymbol{x} - \boldsymbol{b} \tag{3.5}$$

with $\boldsymbol{A} \in R^{6xm}$, $\boldsymbol{b} \in R^m$. The ith-column of $\boldsymbol{A}$ is $\boldsymbol{a}_i$ and each entry of $\boldsymbol{b}$ equals one. Minimizing the root mean square error corresponds to the minimization of the expression:

$$E_m(\boldsymbol{x}) = \frac{1}{2} \boldsymbol{e}^T \boldsymbol{e} = \frac{1}{2} \boldsymbol{x}^T \boldsymbol{A}\boldsymbol{A}^T \boldsymbol{x} - (\boldsymbol{A}\boldsymbol{b})^T \boldsymbol{x} + \frac{m}{2}. \tag{3.6}$$

In classical (unconstrained) LST fitting, this yields the following system of equations for the determination of the EPFS coefficients $\boldsymbol{x}$:

$$\boldsymbol{A}\boldsymbol{A}^T \boldsymbol{x} = \boldsymbol{A}\boldsymbol{b} \tag{3.7}$$

resulting from the unconstrained optimality condition $\nabla E_m(\boldsymbol{x}) = 0$.

Depending on the uniform distribution of the measured stress points and on the use of the L_2-norm in (3.6), the solution (3.7) of the unconstrained problem can yield physically meaningless results. The inherent physical characteristics of the failure surface must be fulfilled as additional constraints of the problem in equality or inequality form. Obviously, the stress space origin must lie within the EPFS surface. This is equivalent to the constraints:

$$H_{11} \geqq 0, \quad H_{22} \geqq 0, \quad H_{33} \geqq 0. \tag{3.8}$$

We assume also that the strongest uniaxial compression resistance is higher than the corresponding tensile resistance in the direction 3. Then, it is valid that:

$$h_3 \geqq 0. \tag{3.9}$$

Relations (3.8) and (3.9) are written in the general linear inequality system form, as follows:

$$\boldsymbol{C}\boldsymbol{x} + \boldsymbol{d} \geqq \boldsymbol{0} \tag{3.10}$$

with $\boldsymbol{d} = \boldsymbol{0}$ and $\boldsymbol{C} = \boldsymbol{I}$.

So far the determination of $\boldsymbol{x}$ amounts to the solution of the constrained minimization problem:

$$\text{Find } \boldsymbol{x} \text{ minimizing } E_m(\boldsymbol{x}) = \frac{1}{2} \boldsymbol{x}^T \boldsymbol{A}\boldsymbol{A}^T \boldsymbol{x} - (\boldsymbol{A}\boldsymbol{b})^T \boldsymbol{x}$$
$$\text{subjected to } \boldsymbol{C}\boldsymbol{x} + \boldsymbol{d} \geqq \boldsymbol{0}. \tag{3.11}$$

Relation (3.11) constitutes a classical Quadratic Programming Problem (QPP) and can be solved through one of the well-established solution techniques. One popular method is the transformation of the QPP (3.11) to the equivalent Linear Complementarity Problem (LCP) and the application of a respective solution algorithm. Setting the inequality constraints as follows:

$$w(\boldsymbol{x}) = \boldsymbol{C}\boldsymbol{x} + \boldsymbol{d}, \quad w(\boldsymbol{x}) \geqq \boldsymbol{0} \tag{3.12}$$

the Lagrangian of the constrained optimization problem (3.11) takes the following form:

$$L(\boldsymbol{x}, \boldsymbol{z}) = E_m(\boldsymbol{x}) - \boldsymbol{z}^T \boldsymbol{w}(\boldsymbol{x}) \tag{3.13}$$

where $\boldsymbol{z}$ lists the Lagrangian multipliers for the inequality side conditions.

The Kuhn-Tucker optimality conditions for the inequality constrained problem (3.11) now take the form:

$$\nabla_x L(\boldsymbol{x}, \boldsymbol{z}) = 0, \quad \boldsymbol{z} \geqq \boldsymbol{0}, \quad \boldsymbol{w}(\boldsymbol{x}) \geqq \boldsymbol{0}, \quad \boldsymbol{z}^T \boldsymbol{w}(\boldsymbol{x}) = 0. \tag{3.14}$$

The first one becomes:

$$\boldsymbol{A}\boldsymbol{A}^T \boldsymbol{x} - \boldsymbol{b} - \boldsymbol{C}^T \boldsymbol{z} = \boldsymbol{0}$$

and yields the desired estimation of $\boldsymbol{x}$ as function of the Lagrangian multipliers, i.e.:

$$\boldsymbol{x} = \boldsymbol{x}_0 + (\boldsymbol{A}\boldsymbol{A}^T)^{-1} \boldsymbol{C}^T \boldsymbol{z}, \quad \text{where} \quad \boldsymbol{x}_0 = (\boldsymbol{A}\boldsymbol{A}^T)^{-1} \boldsymbol{b}. \tag{3.15}$$

$\boldsymbol{x}_0$ is the so-called **"bilateral estimation"** corresponding to (3.7), i.e. the estimation obtained, if the inequality constraints are ignored. Relations (3.12) and (3.15) yield the inequal constraints as linear functions of the Lagrangian multipliers, i.e.

$$\boldsymbol{w} = \boldsymbol{M}\boldsymbol{z} + \boldsymbol{q}, \quad \boldsymbol{w}(\boldsymbol{z}) \geqq \boldsymbol{0} \tag{3.16}$$

with

$$\boldsymbol{M} = \boldsymbol{C}(\boldsymbol{A}\boldsymbol{A}^T)^{-1} \boldsymbol{C}^T, \quad \boldsymbol{q} = \boldsymbol{d} + \boldsymbol{C}\boldsymbol{x}_0. \tag{3.17}$$

Using the rest of the Kuhn-Tucker conditions (3.14), (3.16) and (3.17) the equivalent LCP is obtained:

$$\boldsymbol{z} \geqq \boldsymbol{0}, \quad \boldsymbol{w}(\boldsymbol{z}) \geqq \boldsymbol{0}, \quad \boldsymbol{z}^T \boldsymbol{w}(\boldsymbol{z}) = 0, \quad \boldsymbol{w}(\boldsymbol{z}) = \boldsymbol{M}\boldsymbol{z} + \boldsymbol{q}. \tag{3.18}$$

Now the parameter identification problem amounts to find a solution $\boldsymbol{z}$ of (3.18). Then, (3.15) yields the desired estimation $\boldsymbol{x}$. The numerical solution is obtained by the Mangasarian algorithm [9] given in the Appendix.

The following remarks are useful:

i) The rank of $\boldsymbol{A}$ must be at least 6, to assure that $(\boldsymbol{A}\boldsymbol{A}^T)$ is invertible. i.e. at least 6 measurement points, not lying on a plane, are required. Under this condition $\boldsymbol{M}$ is positive definite and the solution of (3.18) is unique.

ii) The technique described is based on the linearity of the error, as function of the unknown failure criterion coefficients (Eq. (3.3)). The same method is in principle applicable with one basic difference to the Tsai-Wu criterion, but not applicable to the Tsai-Hahn one. The difference is that the ellipticity conditions must be included as a subsidiary condition. The condition is non-linear and thus additional numerical difficulties arise. Moreover, no uniqueness of the solution is assured. Furthermore, if the H_{ij} $(i \neq j)$ is not posed equal to zero to the Tsai-Wu criterion the unknowns become 9 and thus more measurement points are required than for the EPFS criterion, which in any case do not guarantee a uniqueness of the solution. On the other hand, the Tsai-Hahn criterion leads to non-linear error functions with unpredictable effects on the uniqueness and stability of the solution of the parameter identification problem. As a result in the parameter identification problem for failure surface, the EPFS criterion represents the most balanced choice.

These conceptual weaknesses of the popular Tsai-Wu and Tsai-Hahn criteria should be added to the inherent drawbacks of these criteria which either violate phenomenological principles of mechanics, or constitute crude approximations, which may give unacceptable results when applied to real materials [2].

iii) The final value of the error vector given in (3.4) is expressed by:

$$\boldsymbol{e} = \boldsymbol{e}_0 + \boldsymbol{A}^T(\boldsymbol{A}\boldsymbol{A}^T)^{-1}\,\boldsymbol{C}^T\boldsymbol{z}, \quad \text{with} \quad \boldsymbol{e}_0 = \boldsymbol{A}^T\boldsymbol{x}_0 - \boldsymbol{b} \tag{3.19}$$

where $\boldsymbol{e}_0$ is the bilateral error vector.

iv) The mean square deviation, i.e. the cost functional of the constrained minimization problem (3.11) is given by:

$$E_m = E_{mo} + \frac{1}{2}\boldsymbol{z}^T\boldsymbol{M}\boldsymbol{z} \tag{3.20}$$

where E_{mo} is the bilateral mean square deviation. Due to the positive definiteness of $\boldsymbol{M}$, the consideration of the inequality constraints increases the final mean square deviation.

4 The neural network approach to the evolution of the failure surface

By means of the method of Section 3 one can determine the coefficients of the failure surface if certain experimental results are given. We can construct some approximations on the previous, or further evolution of the failure surface by "teaching" the computer to "imitate" the experimental procedure. This is possible by embedding the problem in a neural network environment and by applying a supervised learning algorithm, [10], [11], [12].

Suppose that we have a set of failure measurements and we have constructed the failure surfaces which correspond to them. We would like to extrapolate or interpolate them, in the sense that we give certain failure stress states and we would like to determine the failure surface to which they belong. The failure surfaces sought may lie either "between" the obtained ones by experiments, by applying the method of the previous Section or "beyond" the obtained ones. This kind of prediction of the geometry of the failure surface is possible by using a supervised learning technique, [10], [11].

Neural network models are efficient in computational problems, where many assumptions have to be satisfied in parallel. This is achieved by using networks of neurons with nonlinear behaviour and with a high degree of interconnection. The neurons are connected with links of variable weights. A neural network is defined by the responses of its nodes, the learning rule and the network geometry. The learning rules improve the network total response through adaptive changes of the weights of the links. In the neural network each node (neuron), i, sums up the weighted inputs, say:

$$V_i = \Theta_i + \sum_{j=1}^{n} T_{ji}V_j \tag{4.1}$$

where T_{ji} is the weight of each link or synapse between the i and j neurons, V_j is the output of the j-neuron ($j = 1, \ldots, n$), from all the n-nodes with which it is connected, and gives as an output the quantity:

$$f_i\left(\sum_{j=1}^{n} T_{ji}V_j + \Theta_i\right) \tag{4.2}$$

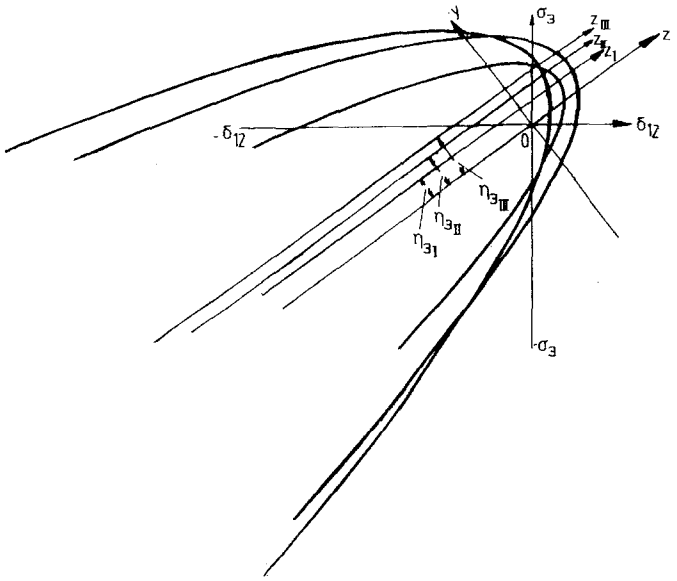

Fig. 1. The principal diagonal plane (σ_3, δ_{12})-intersections of the EPFS for three typical loading steps of the Naxian marble

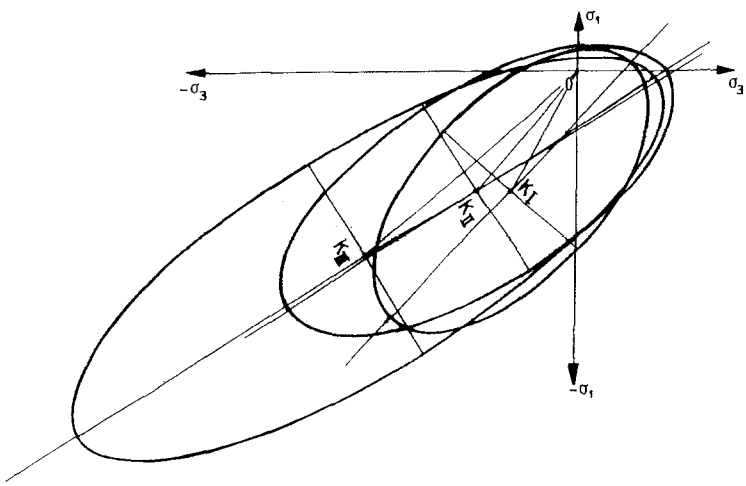

Fig. 2. The (σ_1, σ_3)-principal stress plane intersections of the EPFS for three typical loading steps of the Naxian marble

where $f(.)$ is generally a nonlinear response function. Quantity Θ_i is a real number denoting the external threshold of the i-neuron. In Fig. 1 of [7] we give four common types of f: the **hard limiter** (Fig. 1 a), the **simple limiter** (Fig. 1 b), the **sigmoidal nonlinear limiter** (Fig. 1 c), and the **comparator** (Fig. 1 d). The output of the i-neuron in Fig. 2 in the same references [7] is transmitted to other neurons until a final state of the network is achieved. Here we ***"construct"*** a fictitious neural network, appropriate for the treatment of the posed problem. The proposed neural network and the process of transmission from neuron to neuron is simulated in our problems on a digital computer, since neural computers are not yet available for the moment in the commerce.

Variations of the synaptic weights, according to an adaptive algorithm, endow the neural networks with "learning" capabilities, i.e. that desired outputs may be produced, or approxima-

ted, with any prescribed degree of accuracy. Here we present first an adaptive network called ***adaline*** and then a modification of it, called the ***perceptron***, which will be used for the numerical treatment of the EPFS determination problem.

The adaline (adaptive linear neuron) consists of the neuron of Fig. 2 of [7] which has the possibility to change its weights T_{ji}. More precisely, it consists of an ***adaptive linear combiner*** (ALC), connected with a ***two-level quantizer*** (i.e. f_2, in Fig. 2, is the hard limiter nonlinearity). We replace Θ_j by considering an additional neuron having $T_{j0} = 0$ and $V_0 = 1$. The adaline has $(n + 1)$ inputs $V_0 = 1, V_1, \ldots, V_n$ and two outputs, that is an analog output u_j and a binary output y_j.

Here $u_j = \sum_{i=0}^{n} T_{ji} V_i$ and $y_j = \{+1, \text{if } u_j > 0, \text{ while } -1, \text{if } u_j < 0\}$. The desired output d_j, which is given, is compared with u_j, and the square error $e_j^2 = (d_j - u_j)^2$ is minimized by adjusting the weights T_{ji}. Let us now minimize the square error at the "moment t", given by:

$$E_j = \frac{1}{2} e_j^2(t) = \frac{1}{2} (d_j - u_j)^2. \tag{4.3}$$

We apply the steepest descent minimization algorithm, and we may write the system of differential equations [10] as follows:

$$\frac{dT_{ji}}{dt} = -\mu \frac{\partial E_j}{\partial T_{ji}} = -\mu \frac{\partial E_j}{\partial u_j} \frac{\partial u_j}{\partial T_{ji}} \qquad \mu > 0. \tag{4.4}$$

Then, from $u_j = \sum_{i=0}^{n} T_{ji} V_i$ we obtain that:

$$\frac{dT_{ji}}{dt} = \mu \left[d_j - \sum_{r=0}^{n} T_{jr} V_r \right] V_i \tag{4.5}$$

where $\mu > 0$ is called the ***learning parameter***, or the ***adaptive gain***. Through "time" discretization (4.5) yields:

$$T_{ji}^{(k+1)} = T_{ji}^{(k)} + \eta^{(k)} (d_j - u_j^{(k)}) \, V_i^{(k)} \qquad k = 0, 1, 2, \ldots \tag{4.6}$$

which is the Widrow-Hoff "Delta Rule" for learning [13].

Here $0 < \eta^{(k)} < \eta_{\max}$ is the learning rate, which controls the convergence and stability of the weight adaption process. Concerning the choice of the constant, $\eta^{(k)}$, and the logic functions which can be realized by a single adaline after training, see [10]. Figure 3 of [7] gives the adaline neural network.

The perceptron is analogous to the adaline with the only difference that $u_j = \sum_{i=0}^{n} T_{ji} V_i$ is sent through a quantizer of the type of hard limiter, i.e. $y_j = \text{sign } u_j$. Thus, a binary output $y_j = \pm 1$ is obtained. This output is compared with the desired output d_j, which is given also in binary form, i.e. $d_j = \pm 1$. Then, the quantized error $e_j = d_j - y_j$ is considered for the adjustment of the weights. For the perceptron the learning rule reads:

$$T_{ji}^{(k+1)} = T_{ji}^{(k)} + \eta e^{(k)} V_i^{(k)}. \tag{4.7}$$

Here $y_i^{(k)} = \text{sign } u_j^{(k)}$, $\tilde{e}_j^{(k)} = \tilde{d}_j^{(k)} - y_j^{(k)}$ and $u_j^{(k)} = \sum_{i=1}^{n} T_{ji}^{(k)} V_i^{(k)}$. Index (k) denotes the time moment, as in (4.6). In many problems it is better to replace the hard-limiter function by

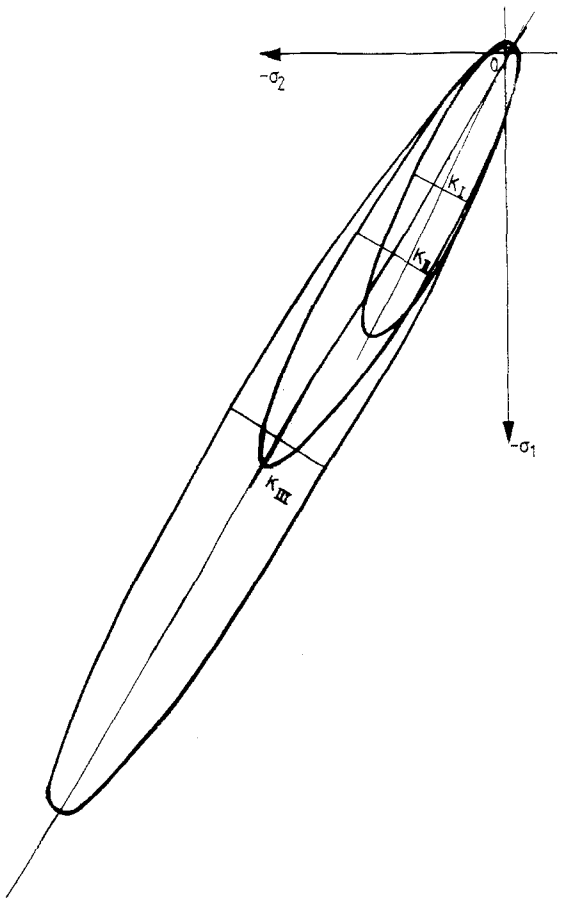

Fig. 3. The (σ_1, σ_2)-principal stress plane intersections of the EPFS for three typical loading steps of the Naxian marble

a sigmoid function, i.e. $y_j = \tanh(\gamma u_j)$, $\gamma > 0$. Then, the steepest-descent algorithm yields that [10]:

$$T_{ji}^{(k+1)} = T_{ji}^{(k)} + \eta\gamma\tilde{e}_j^{(k)}[1 - (y_j^{(k)})^2]\, V_i^{(k)}. \tag{4.8}$$

A generalization of the single-layer perceptron is the multilayer perceptron.

The problem, which we have to solve is the following: Suppose that we dispose various loading paths through given stress states lying on a prescribed failure surface. The ends of the paths (in the case of extrapolation) or certain intermediate points of the paths (in the case of interpolation) are given and they belong to distinct failure surfaces, which must be determined. This is again a parameter identification problem analogous to the one of ref. [7].

In a neural network environment the parameter identification problem can be formulated as a ***"supervised learning"*** problem. The learning is called supervised because it is guided by taking into account the desired result. Suppose now that the stresses, σ, are prescribed. We want to determine the control vector $z = \{H_{11}, H_{22}, H_{33}, h_1, h_2, h_3\}$ such as to minimize the differences in (4.3) (d_j are the given stress states). For the numerical solution we apply a scheme analogous to (4.6). The determination of the values of the EPFS coefficients is achieved by means of an adaline neural network N, in which the H_{ii}, h_i $(i = 1, 2, 3)$ represent the synaptic weights. The network operates in the following way: The initial guess $z^{(0)}$ gives an initial estimation of the failure surface, which is intersected by the path in the point $\sigma^{(0)}$.

Then, we transmit $z^{(0)}$ to the adaline N and we adopt the following iterative scheme (cf. also (4.6)):

$$H_{ii}^{(1)} = H_{ii}^{(0)} + \eta^{(0)} g \left[\sum_{i=1}^{3k} \left(\sigma_i - \sum_{\iota=1}^{3} H_{i\iota}^{(0)} \sigma_\iota^{(0)} \right) \sigma_\iota^{(0)} \right] \tag{4.9}$$

$$h_i^{(1)} = h_i^{(0)} + \eta^{(0)} g \left[\sum_{i=1}^{3k} \left(\sigma_i - \sum_{\iota=1}^{3} h^{(0)} \sigma_\iota^{(0)} \right) \sigma_\iota^{(0)} \right]. \tag{4.10}$$

Here g is a function (e.g. of the type of Fig. 1 c of [7]) indicating the correcting term influence, and k denotes the number of triads of stresses σ_1, σ_2, σ_3 in the principle stress space, which are the prescribed stress states belonging (or at least lying very close) to the sought interpolated or extrapolated failure surface.

The convergence theory for the perceptron [13] implies here that, if the learning problem which we study has a solution, the perceptron algorithm converges to this solution.

5 Numerical applications

Experimental studies on the subsequent yield surfaces of engineering materials have been reported by extremely numerous investigators. It may be stated that the experimental study of yield loci of ductile and semibrittle materials constitutes the experiment which occupied most the interest of research for many decades of years and various laboratories. Some important contributions to this subject are reviewed in the literature [14], [15]. However, all these important studies are restricted to the determination of only some of the elastic and plastic properties of the deformed material and they do not yield the complete number of stress limits for each loading step along the principal directions of anisotropy of the material. Thus, these tests, although very important, do not give all the necessary informations for the unambiguous definition of the successive yield loci of the deformed material, which as the loading is progressing are changing in anisotropy due to the evolution of plasticity and the strength differential effect.

Therefore, in our studies here, in order to study the possibilities of the method we are utilizing data from experiments, which, due to their completeness, directness and accuracy, may assure the safe and accurate definition of the failure loci at each loading step. These experiments are with a coarse-grained dense crystalline marble of an excellent quality from the Greek island of Naxos, extensively used in engineering constructions, as well as in artistic applications. This kind of marble presents a cataclastic mode of deformation, since it is a rock derived from igneous parent rocks, in which the mineral grains have a highly oriented fabric of the schist type, and in which needle-like or platy minerals tend to lie with their long directions parallel, or their planar directions parallel, so that they present a pronounced mineralogical layering. This particular layering influences the mechanical properties of the rock and it will be also detected by the mode of anisotropy of the material, revealed during the applications of loads in triaxial tests.

This kind of the material presents an early defined system of principal directions of anisotropy, where the direction normal to the platy and needle-like inclusions is always a principal stress direction, whereas the other two principal directions lie on the platy inclusions parallel and normal to the needle-like inclusions. Furthermore, the strength of this material is rather reduced, so that modern triaxial testing machines can satisfactorily load the specimens up to fracture. Therefore, it was decided to use this type of material for applying the method developed in the paper and take into consideration the existing accurate experimental results existing in the literature [16]. However, the elasto-plastic behaviour of this material does not

differ in principle with any mildly ductile material (metal or other material), and therefore the results of application of the method on such a material should be considered as of a general validity.

The specimens used in our tests have a prismatic form of a length of 10 cm and a cross-section 5×5 cm^2, which are considered as eliminating most of the end-effects in their central parts, where measurements of strains were performed. Triaxial tests under constant levels of the one lateral component of the principal stresses (σ_2) gave the following results contained in Table 1. Repetition of identical tests has shown that reproducibility was satisfactory in the loading-unloading cycles, employed to determine a recoverable strain behaviour at different loading steps. These tests were used to define initial and subsequent yields of the material, which were, however, different for different loading paths, depending on the differences of the intermediate stresses.

In engineering applications, under arbitrary modes of external triaxial loading, it is sufficient to assume that the material is in principle a generally orthotropic material, since materials utilized in engineering constructions do not usually exceed this degree of anisotropy. In order to

Table 1. The values of the yield stresses under triaxial loading from parametric values of the σ_i-principal stress at three loading steps (initial yielding, conventional yielding at $e = -0.002$ and yielding at ultimate strength) of a Naxian marble

σ_1	σ_2	σ_{3y}	$\sigma_{3y}(\varepsilon = -0.2\%)$	σ_{3u}
0	3.50	49.00	52.30	60.70
	10.34	62.00	68.00	76.90
	20.70	73.50	79.90	105.00
	34.45	78.10	96.00	105.30
3.50	3.50	52.70	55.00	65.30
	5.20	53.80	71.50	75.10
	6.90	65.60	79.50	83.90
	10.35	70.20	116.20	94.10
	27.60	95.80	170.40	129.80
	69.00	116.70	143.30	192.20
	82.75	103.10	–	143.30
6.90	6.90	75.30	–	83.80
	13.80	85.30	96.60	112.80
	27.60	101.40	–	134.10
	55.20	137.80	186.50	191.60
	82.75	135.10+	188.10	188.10
	110.30	129.10+	137.80+	174.60
13.80	13.80	80.00	115.50	115.90
	20.70	94.40	117.20	126.30
	27.60	112.10	141.70	147.70
	41.40	126.00	150.80	154.80
	55.20	145.90+	189.20	196.40
	82.75	169.60+	235.70	254.40
	110.30	225.90	267.50	278.10
20.70	20.70	105.80	138.00	138.00
	27.60	118.70	145.00	150.20
	62.05	156.10	–	208.70
	82.75	205.30+	259.40	260.20
	110.30	191.20	288.00	289.10

run a series of complicated triaxial tests a combination of two loading machines was used. The first was capable to apply an axial load of up to 2,000 KN, whereas the second could supplement the loading of the specimen by generating a confining pressure through a servocontrolled system, thus loading the piston of the pressure vessel. The latter machine was equipped by a precise and quick-responding servovalve, thus maintaining constant confining pressure inside the triaxial loading cell, when the specimen is either contracted or dilated. The loading unit, consisting of a pressure vessel and the triaxial cell, was designed to sustain pressures up to 250 MPa. The pressure vessel was connected with the triaxial cell, so that the pressure in the vessel was transmitted to triaxial cell with the servomechanism keeping a constant pressure during the test, while lateral volumetric changes in the specimen were transformed into linear movements of the piston. The main characteristics of the testing device are, therefore, a uniformly distributed and independently controlled device of application of a triaxial type of principal stresses, complemented by a system of accurate and rapidly measured strains in a large range of deformations, whereas the machine is a robust one, which disposes a high capacity of sustaining stresses of the order of 250 MPa.

For establishing the strength behaviour of this type of brittle rock under a triaxial mode of loading, a series of tests were conducted along loading paths following either the hydrostatic axis in the stress space, or paths with varying $\sigma_2 = \sigma_3$ stresses, while the σ_1-principal stress was kept constant, or path in which the σ_1- and σ_2-stresses are kept constant at various levels and increased the σ_3-stress up-to-yielding and ultimate strength of the material. Tables 1 and 2 present the variation of the σ_1, σ_2, σ_3, components of principal stresses, either at initial yielding, or at a conventional yielding creating a volumetric conventional strain $\varepsilon_{vol} = -0.2\%$, or at peak strength [16]. Initial yielding is defined according to the ASTM standards as a minimum deviation from linearity of the stress-strain curve of the material in simple tension.

Table 2. The values of the yield stresses under triaxial loading from parametric values of the σ_2-principal stress at three loading steps (initial yielding, conventional yielding at $e = -0.002$ and yielding at ultimate strength) of a Naxian marble

σ_1	σ_2	σ_{3y}	$\sigma_{3y}(\varepsilon = -0.2\%)$	σ_{3ult}
0	20.70	73.5	79.9	105.0
13.80		94.4	117.2	126.3
20.70		105.8	138.0	138.0
3.45	27.60	95.8	170.4	129.8
6.90		101.4	–	134.3
13.80		112.1	141.7	147.2
20.70		118.7	145.0	150.2
27.60		122.4	160.0	170.0
6.90	55.20	137.8	186.5	191.6
13.80		145.9	189.2	196.4
27.60		165.6	188.9	222.0
55.15		192.0	244.3	–
3.45	82.75	103.1	128.4	143.3
6.90		135.1	188.1	188.1
13.80		169.6	235.7	254.4
20.70		205.3	249.4	260.2

The results from triaxial tests included in Table 1 and 2 are obtained as follows: The one of the lateral principal stresses, either the σ_1-stress, for Table 1, or the σ_2-stress, for Table 2, were kept constant at different loading steps. Then, combinations of the two remaining principal stresses σ_2 and σ_3 for Table 1 and σ_1 and σ_3 for Table 2 define the respective yield limits for the three different loading steps.

By applying the method of Section 3, we identify the failure surfaces of EPFS corresponding to the data (a) of the initial yield column of Table 1 which we call the (first quadric), (b) the $\varepsilon^P = -0.2‰$ yield strain column of the same Table where ε^P is the strain which corresponds to the initiation of the conventional plastic flow. This failure surface is called the second quadric and (c) the peak strength column of the same Table, which is called the third quadric.

For the application of the method we consider as given the experimental yield points on the failure surfaces for subsequent loading steps inside the elastic-plastic region of loading and unloading of the specimens. On each given yield surface we take a finite number of points $\sigma_{ij} = (i = j = 1, 2, 3)$ and we apply with respect to all given yield surfaces the numerical procedure of the previous Section. We assume that the elastic material is orthotropic, of changing anisotropy with loading, and we want to determine the sequence of the orthotropy coefficients $\alpha_{11}^{(\varrho)}, \alpha_{22}^{(\varrho)}, \alpha_{12}^{(\varrho)} = \alpha_{21}^{(\varrho)}, \alpha_{33}^{(\varrho)}$, within each element, which satisfy the identification problem for the stresses and constitute the elasticity tensor $C^{(\varrho)}$ at the ϱ-step of the learning algorithm. As $\varrho \to \infty$ we theoretically obtain the solution tensor $C = \{\alpha_{11}, \alpha_{22}, \alpha_{12} = \alpha_{21}, \alpha_{33}\}$. We recall here that $\varepsilon_x = \alpha_{11}\sigma_x h + \alpha_{12}\sigma_y h, \ldots, \gamma_{xy} = \alpha_{33}\sigma_{xy} h$, where $h = 1$ mm is the thickness of the plane structure. The yield point is defined by the limit stress, which corresponds to a plastic strain of 0.02 percent, [14], [15].

In order to get a more reliable approximation of the anisotropic elastoplastic problem with a sequence of anisotropic elastic problems, we also have considered intermediate yield points, through interpolation between two experimentally given failures in the 3D-stress space. The interpolation is guided by assuming that the stress point lies always on an elliptic paraboloid failure surface, for the general anisotropic hardening elastoplastic body presenting the strength differential effect [1], [2]. The failure surface in any principal stress plane is an ellipse, which can be defined from a series of points. The same property is valid for the deviatoric plane, as well as for any intersection parallel to this plane. The only exception to the general rule holding for the (EPFS)-criterion is for intersections of the failure paraboloid by planes containing the hydrostatic axis or the axis of symmetry of the paraboloid. These intersections are all parabolas [1], [2]. After the initial rough guess of a family of yield surfaces from a series of different experimentally determined triads of values of the principal stresses leading to different points of presumably the same yield surface, we obtain a family of slightly different failure loci corresponding to equivalent steps, but of different loading paths in the three dimensional principal stress space.

The above procedure may be applied to obtain also subsequent yield surfaces for further loading and unloading steps from the experimental ones, for which the subsequent yield surfaces are known. Again, we determine a number of stress points, now by extrapolation, and we pass through these points an elliptic paraboloid failure surface in the respective $(\sigma_1, \sigma_2, \sigma_3)$ principal stress space, corresponding to this loading step. One should notice that the calculated orthotropic coefficients are fictitious and they are not uniquely determined.

The three loading steps of the Naxian marble tested included in Tables 1 and 2 gave finally the following values for the terms of the respective tensors H_{ij} and h_i, contained in Table 3 a. Having at our disposition these values of stresses and of the coefficients H_{ij} and h_i, we can readily define the various intersections of the failure hyperspaces.

It may be readily shown [1], [2] that the intersections of the failure hyperspaces by the three principal diagonal planes (σ_3, δ_{12}), (σ_1, δ_{23}) and (σ_2, δ_{13}) are all parabolas, whose axes of symmetry are parallel to the 0z-hydrostatic axis and lying at different distances from it, as the loading is progressing inside the plasticity zone. Their equations are derived from relation (2.9) by a cyclic interchange of the respective indices. It has been proved that the EPFSs for the general orthotropic material have their axes of symmetry parallely displaced, relatively to the hydrostatic axis, but moving outside the principal diagonal planes. Indeed, for the orthotropic materials the respective EPFSs are angularly displaced, so that the

Table 3. The values of the terms of the elliptic paraboloid failure surface, (a) as well as the values of the characteristic quantities defining the (σ_1, σ_2), (σ_1, σ_3), and (σ_2, σ_3) principal stress intersections for the EPFSs (b, c, d)

(a)

Loading steps	H_{11}	H_{22}	H_{33}	h_1	h_2	h_3	Remarks
Elastic limit (I)	0.19380	0.63794	0.21215	36.0586	0.12897	0.19375	All H_{ij} & h_i must be multiplied by $(x10^{-3})$
Initial yielding (II)	0.16969	0.42635	0.09545	27.743	0.11351	0.15328	
Ultimate strength (III)	0.34174	0.85537	0.15794	60.919	0.13114	0.14247	

(b)
Principal stress plane $(\sigma_1, \sigma_2)^{(*)}$

Loading steps	σ_{1M}	σ_{2M}	$\lambda_{12}{}^{(**)}$	r_{12}	a_{2M}	a_{1M}	$\theta_{12}{}^{(**)}$
Elastic limit (I)	−416.54	−202.38	−25.91°	463.10	154.09	202.38	−27.18°
Initial yielding (II)	−611.12	−358.90	−30.42°	708.72	128.04	753.11	−31.43°
Ultimate strength (III)	−1167.38	−709.18	−31.28°	1365.91	176.27	1389.72	−31.85°

(c)
Principal stress plane $(\sigma_1, \sigma_3)^{(*)}$

	σ_{1M}	σ_{3M}	$\lambda_{13}{}^{(**)}$	r_{13}	a_{1M}	a_{2M}	$\theta_{13}{}^{(**)}$
Elastic limit (I)	−74.93	−134.87	−47.26°	156.92	184.36	55.48	−42.74°
Initial yielding (II)	−135.85	−113.92	−39.98°	−177.30	256.14	114.00	−57.36°
Ultimate strength (III)	−241.31	−214.71	−24.36°	−323.00	412.14	81.86	−58.66°

(d)
Principal stress plane $(\sigma_2, \sigma_3)^{(*)}$

	σ_{2M}	σ_{3M}	$\lambda_{23}{}^{(**)}$	r_{23}	a_{2M}	a_{3M}	$\theta_{23}{}^{(**)}$
Elastic limit (I)	−1.64	−3.00	−61.27°	−3.42	171.81	35.01	−61.49°
Initial yielding (II)	−1.95	−4.40	−66.10°	−4.81	227.65	44.62	−66.61°
Ultimate strength (III)	−1.53	−3.71	−67.55°	−4.02	210.59	31.78	−68.04°

(*) All stresses in MPa's
(**) Negative angles are measured from the negative principal axes with the lower index

Table 4. The values of the principal stresses in tension (σ_{Ti}) and compression (σ_{Ci}) along the three principal axes for the EPFSs

Loading steps	$\sigma_{T1}{}^{(*)}$	σ_{C1}	σ_{T2}	σ_{C2}	σ_{T3}	σ_{C3}
Elastic (I)	24.54	−210.60	39.49	−39.69	68.20	−69.11
Initial yielding (II)	30.39	−193.88	48.30	−48.56	101.55	−103.16
Ultimate strength (III)	15.10	−193.36	34.11	−34.78	79.12	−80.02

(*) All components of stresses in MPa's

centers of their transverse elliptic intersections lie outside the principal diagonal planes and their symmetry planes are intersecting the pricipal diagonal planes along lines parallel to the hydrostatic axis, whose traces on the deviatoric plane lie outside the origin of coordinates.

Figure 1 presents the parabolas corresponding to the intersections of the failure loci by the (σ_3, δ_{12})-principal diagonal planes. It is obvious from these plottings that, as the loading of the material increases up to its ultimate strength, the elliptic paraboloids become more and more shallow, and the distances of their symmetry axes from the hydrostatic axis increase progressively. It has been already shown that, when the anisotropy of the material is increasing, its representative failure locus becomes progressively shallower and the coordinates η and ξ of the distances between the symmetry axis of the paraboloids and the hydrostatic axis are also increasing. These distances for the orthotropic material are given by complicated relationships for the general orthotropic material and they are not given here. These relationships for the transversely isotropic material are considerably simplified and they are given in [2].

The principal stress intersections of the elliptic paraboloid failure surfaces which are of most interest because they give the respective failure loci in the principal stress planes are elliptic curves whose centers are the following coordinates [2] and an angle λ_i of inclination of the polar radii of their centers given by:

$$(\sigma_{3M}, \sigma_{1M}) = \left\{ \frac{\frac{1}{2}(h_3 H_{31} - h_1 H_{33})}{(H_{11} H_{33} - H_{31}^2)}, \frac{\frac{1}{2}(h_1 H_{31} - h_3 H_{11})}{(H_{11} H_{33} - H_{31}^2)} \right\} \tag{5.1}$$

$$\lambda_1 = \frac{\arctan (h_1 H_{33} - h_3 H_{11})}{h_3 H_{33}}. \tag{5.2}$$

The systems of Cartesian coordinates $(M - \sigma_1, \sigma_3)$, to which these ellipses are central and symmetric, are defined by the angles θ_1, expressed by:

$$\theta_1 = \frac{1}{2} \arctan \left(\frac{2H_{31}}{H_{33} - H_{11}} \right) \tag{5.3}$$

whereas the semi-axes a_{1M} and a_{3M} of the ellipses are given by:

$$a_{1M}, a_{3M} = \frac{\sqrt{\frac{1}{a}}}{\sqrt{\frac{1}{b}}} \sqrt{1 + \frac{H_{11} h_3^2 + H_{33} h_1^2 - 2h_1 h_3 H_{31}}{(H_{11} - H_{22})^2 + H_{33}(4H_{12} - H_{33})}} \tag{5.4}$$

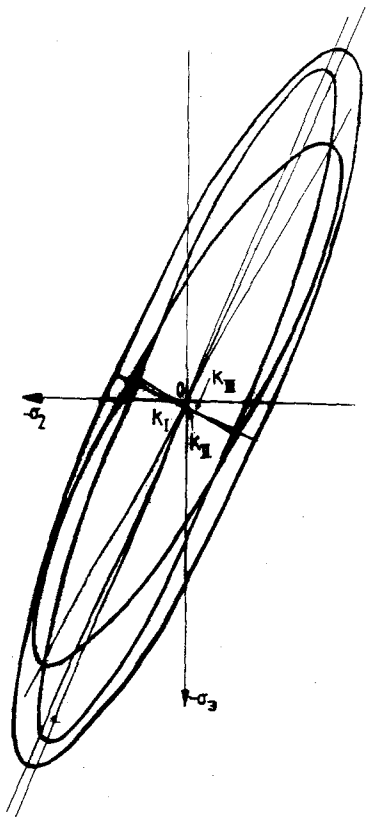

Fig. 4. The (σ_2, σ_3)-principal stress plane intersections of the EPFS for three typical loading steps of the Naxian marble

where:

$$\bar{a}, \bar{b} = \frac{1}{2}\left[(H_{11} + H_{33}) - \sqrt{(H_{33} - H_{11}^2) + 4H_{31}^2}\right]. \tag{5.5}$$

Similar relationships are valid for the two other principal stress planes ((σ_1, σ_2) and (σ_2, σ_3)), where these equations are established by cyclic rotation of the indices.

Table 3 (b, c, d) contains all the necessary dimensions for plotting these intersections. Thus, the σ_{iM}, σ_{jM} coordinates of the centers of the ellipses, as well as their polar distances for the origin 0 are given complemented by the polar angles λ_{ij}, of these polar distances. Similarly the principal semi-axes of the ellipses are given together with the orientation of their major axes relatively to the principal frames of the EPFS. Furthermore, Figs. 2–4 present these intersections for the Naxian marble tested. Table 4 gives the values of principal stresses in tension and compression along the principal directions of the simple substance when it is loaded at the three loading steps considered in this paper.

6 Results

The neural network learning approach developed in this paper to solve a parameter identification problem for the mode of failure of anisotropic materials was employed to solve the general elastoplastic problem under multiaxial loading. The procedure succeeded to solve

completely the problem of the definition of the failure loci of a material deformed progressively in the elastic, up to its ultimate strength, by using only experimental data concentrated in a small area of the yielding, conveniently selected to give reliable and accurate experimental data. In this paper three characteristic steps of loading of a granular rock were considered, that is, in its elastic range, in the initial yielding defined by an effective strain of 0.02%, and finally at its ultimate strength. The experimental data were all concentrated in the compression-compression-compression octant of the yield locus, where these tests could be effectively executed. The method succeeds to yield a full picture of the failure hypersurface of the material, based on data belonging in the underbelly of the respective yield loci.

The parameter identification method, realized in an appropriate neural network environment, through supervised and unsupervised learning algorithms presents certain definite advantages over the classical numerical analysis with adjoining constraints, since it is derived from applying optimization problems, based on a neural network approach, where the anisotropic hardening elastoplastic behaviour is approximated by an ideal convenient material, whose properties are adapted to the existing experimental data. This method will be the subject of a companion paper.

It is clear from Figures 1 to 4 that the material is strongly anisotropic with variable anisotropy, if the material is loaded inside the plastic zone. Moreover, the compression strength of the material is very pronounced and increasing as the loading is progressing. Table 4 indicates the values of the yielding stresses in triaxial loading, as the loading is progressing. Examining the values of the terms h_i, responsible exclusively for the strength differential effect, one observes the striking difference between the values of h_1 and, on the other hand, the respective values of h_2 and h_3. These values are a hundred times smaller than h_1 and almost equal. This phenomenon indicates that the strength differential effect at the plane (σ_2, σ_3) of symmetry is insignificant. Figure 4 indicates the same phenomenon. The three elliptic intersections by the (σ_2, σ_3)-plane of the EPFSs at different steps of loading have their centers almost at the origin 0 of the coordinate system $\sigma_2 0 \sigma_3$, thus resulting to almost equal tension and compression stresses along the principal axes of the ellipses.

Appendix: The Mangasarian algorithm

The Mangasarian successive relaxation technique is a simple and powerful technique for solving symmetric LCPs, consisting of a number of iteration circles in the sense of the well-known Gauss-Seidel method. Within each iteration, the side conditions are set sequentially equal to zero to yield an estimation of the respective Lagrangian multiplier. If this one is nonnegative, it is retained; otherwise, it is set to zero and the gap values are suitably updated. A computer-oriented implementation is described next.

Let ω denote the relaxation parameter $(0 < \omega < 2)$. In the sequel, m_ϱ will always denote the ϱ-column of the matrix M. Let $m_{\varrho\varrho}$ be the ϱ-diagonal of M. Let us assume that k iterations have been completed and within the $k+1$ iteration the values of j-1 Lagrangian multipliers $s_\varrho{}^{k+1}$, $\varrho = 1, 2, \ldots, j-1$ have been already computed; that is, we are ready to proceed with the computation of the next Lagrangian multiplier $s_j{}^{k+1}$. The current side condition estimates are:

$$w = \sum_{\varrho=1}^{j-1} m_\varrho s_\varrho{}^{k+1} + m_j s_j{}^k + \sum_{\varrho=j+1} m_\varrho s_\varrho{}^k + q.$$

Lagrangian multiplier correction: $\Delta s_j = -\omega w_j / m_{jj}$
Candidate Lagrangian multiplier: $y = s_j{}^k + \Delta s_j$
Final Lagrangian multiplier: If $y < 0$ set $s_j{}^{k+1} = 0$, $c = -s_j{}^k$
else, set $s_j{}^{k+1} = y$, $c = \Delta s_j$
Update side conditions: $\boldsymbol{w} = \boldsymbol{w} + \boldsymbol{m}_j c$.

Acknowledgements

The research contained in this paper has been supported by a research programme no 246 allocated by the research Fund of the Academy and partly supported by the Lilian Boudouris Foundation. The authors express their thanks for this support. They express also their gratitude to Mrs. Anna Zografaki for helping them in typing the manuscript and plotting the figures of the paper. Furthermore, the calculations have been performed in a HP 755 computer of the Institute of Steel Structures, Aristotle University, Thessaloniki, Greece. The authors are acknowledging this help.

References

[1] Theocaris, P. S.: Failure criteria for transtropic pressure dependent materials. Rheol. Acta **27,** 451–465 (1988). See also: Theocaris, P. S.: The paraboloid failure surface for the general orthotropic material. Acta Mech. **79,** 53–79 (1989).
[2] Theocaris, P. S.: Failure criteria for anisotropic bodies. In: Handbook of fatique crack propagation in metallic structures. (Carpinteri, A., ed.) pp. I, 3–45. New York: Elsevier 1994.
[3] Theocaris, P. S., Panagiotopoulos, P. D.: Neural computing and artificial intelligence in fracture mechanics. Proc. Nat. Acad. Athens **66,** 373–400 (1991) (in Greek).
[4] Theocaris, P. S., Panagiotopoulos, P. D.: Neural networks for computing in fracture mechanics. Methods and prospects of applications, Comp. Math. Appl. Mech. **106,** 213–228 (1993).
[5] Kortesis, S., Panagiotopoulos, P. D.: Neural networks for computing in structural analysis. Methods and prospects of applications. Int. J. Num. Meth. Eng. **36,** 2305–2318 (1993).
[6] Avdelas, A. V., Panagiotopoulos, P. D., Kortesis, S.: Neural networks for computing in elastoplastic analysis of structures. Mechanica **30,** 1–15 (1995).
[7] Theocaris, P. S., Panagiotopoulos, P. D.: Generalized hardening plasticity approximated via anisotropic elasticity: A neural network approach. Comp. Math. Appl. Mech. Eng. **125,** 123–139 (1995) See also: Plasticity including the Bauschinger effect, studied by a neural network approach. Acta Mech. **113,** 63–75 (1995), and: Hardening plasticity approximated via anisotropic elasticity. The Fokker-Planck equation in a neural network environment. ZAMM **75,** 889–900 (1995).
[8] Wu, E. M.: Mechanics of composite materials. (Sendeckyj, G. P., ed.), Vol. 2, p. 353. New York: Academic Press 1974.
[9] Mangasarian, O. L.: Solution of symmetric linear complementarity problems. J. Optim. Theor. Appl. **22,** 465–485 (1977).
[10] Cichocki, A., Unbehauen, R.: Neural networks for optimization and signal processing. New York: J. Wiley 1993.
[11] Ritter, H., Martinez, T., Schulten, K.: Neural computation and self-organizing maps. Reading: Addison-Wesley 1992.
[12] Panagiotopoulos, P. D.: Hemivariational inequalities application in mechanics and engineering. Berlin, Heidelberg, New York: Springer 1993.
[13] Beale, R., Jackson, T.: Neural computing. An introduction. Bristol: Adam Hilger 1990.
[14] Ikegami, K.: An historical perspective of the experimental study of subsequent yield surfaces for metals part II. J. Soc. Mat. Sci. **24,** 709–719 (1975).
[15] Shiratori, E., Ikegami, K.: Experimental study of the subsequent yield surface by using cross-shaped specimens. J. Mech. Phys. Solids **16,** 373–394 (1968). See also: Shiratori, E., Ikegami, K., Kaneko, K.: Subsequent yield surfaces determined in consideration of the Bauschinger effect in foundations of

plasticity (Sawczuk, A., ed.) Leyden: Noordhoff 1973, and Shiratori, E., Ikegami, K., Yoshida, F.: Analysis of stress-strain relation by use of an anisotropic hardening plastic potential. J. Mech. Phys. Solids **27,** 213–229 (1979).

[16] Michelis, P. N.: Work softening and hardening behaviour of granular rocks. Rock Mech. **14,** 187–200 (1981).

Authors' addresses: P. S. Theocaris, Institute of Mechanics, National Academy of Athens, P.O. Box 77230 17510 Athens, Greece and C. Bisbos and P. D. Panagiotopoulos, Department of Civil Engineering, Aristotle University of Thessaloniki, Thessaloniki, Greece